Preprint Title	Non-labeled and highly sensitive probe detection with novel hierarchical SERS substrates fabricated by nanoindentation and chemical reaction methods
Authors	Jingran Zhang, Tianqi Jia, Yongda Yan, Li Wang, Peng Miao, Yimin Han, Xinming Zhang, Guangfeng Shi, Yanquan Geng, Zhankun Weng, Daniel Laipple and Zuobin Wang
Publication Date	20 Aug 2019
Article Type	Full Research Paper
Supporting Information File 1	support information.doc; 4.1 MB
ORCID® iDs	Jingran Zhang - https://orcid.org/0000-0002-4258-461X; Yanquan Geng - https://orcid.org/0000-0003-3499-0551; Zhankun Weng - https://orcid.org/0000-0002-0945-9825

Non-labeled and highly sensitive probe detection with novel hierarchical SERS substrates fabricated by nanoindentation and chemical reaction methods

Jingran Zhang[*1], Tianqi Jia[*1], Yongda Yan[2], Li Wang[3], Peng Miao[4], Yimin Han[*5], Xinming Zhang[1], Guangfeng Shi[1], Yanquan Geng[2], Zhankun Weng[1], Daniel Laipple[3], Zuobin Wang[1]

[1] *Ministry of Education Key Laboratory for Cross-Scale Micro and Nano Manufacturing, Changchun University of Science and Technology, Changchun 130022, China*

[2] *The Key Laboratory of Micro-systems and Micro-structures Manufacturing of Ministry of Education, Harbin Institute of Technology, Harbin, Heilongjiang 150080, P.R. China*

[3] *Institute of Materials Research, Helmholtz-Zentrum Geesthacht, Max-Planck-Strasse 1, Geesthacht, D-21502, Germany*

[4] *School of Chemistry and Chemical Engineering, Harbin Institute of Technology, Harbin, Heilongjiang 150010, P.R. China*

[5] *Department of Gynaecology, No. 3 Subsidiary Hospital, Harbin Medical University, Harbin, Heilongjiang, 150040, P. R. China*

** Corresponding author. Tel.: +86-0451-86298932*

E-mail address: hanyimin@163.com *(Y.M. Han)*

** Corresponding author. Tel.: +86-0431-85582420*

E-mail address: zhangjingran@cust.edu.cn *(J. R. Zhang)*

Abstract

Nanostructures and nanoparticles are two typical structures which have already been widely employed as the Surface Enhanced Raman Scattering (SERS) substrates. In most studies, they are employed separately as SERS substrates. Recently, the hierarchical structures including nanostructures and nanoparticles present better SERS characteristics. However, how to machine such hierarchical structures is a big problem. In the present study, a novel method integrating the nanoindentation process and chemical redox reaction to machine the hierarchical SERS substrate is provided. Micro/nanostructures are formed on the Cu(110) plane first, and then Ag nanoparticles are generated on the structured Copper surface. Effects of parameters of the indentation process and the corrosion times in the $AgNO_3$ solutions on the Raman intensities of the SERS substrate with hierarchical structures are experimentally studied. The intensity and distribution of the electric field of single and multi Ag nanoparticles on the surface of plane and micro/nanostructures are studied with the COMSOL software. The feasibility of the hierarchical SERS substrate is verified using R6G molecules. Finally, the enhancement factor of malachite green molecules can reach to 5.089×10^{9}, which proves that the method is simple, replicable and low cost method for machining the hierarchical SERS substrate.

KEYWORDS: Ag nanoparticles, nanostructures, R6G, malachite green molecules, SERS, hierarchical substrates

Introduction

SERS has triggered a lot of research interest due to its suitability as an analytical tool for the ultrasensitive detection of molecules [1-4]. Compared to traditional Raman scattering technology, SERS is a surface phenomenon associated with the amplification by several orders of Raman intensity for analyte molecules. The high resolution results from the combination of chemical (CM) [5] and electromagnetic enhancement (EM) [6,7]. The CM enhancement is main factor for charge transfer between SERS substrate and probe molecule. The EM field enhancement is main factor for localized surface plasmon resonance and significantly depends on the induced near-field intensity. The size, shape, interparticle spacing of the nanoparticles or nanostructures influence the LSPR. A series of metals including Au, Cu and Ag are useful in ultra-trace biological or chemical sensing and have shown a huge amount of potential to obtain surface enhancement. Thus different nanoparticles or micro/nanostructures become a SERS sensor to detect adsorbed markers.

Generally, nanoparticles are fabricated as SERS substrates with low cost and high production by using chemical synthesis methods [8-13], including chemical/electrochemical deposition, electrochemical etching. For instance, Chen et al. [8] employed electrochemical etching method to fabricate nanocube structures on the $Cu_{30}Mn_{70}$ surface by controlling the voltage. In addition, Zhang et al. [10] showed that gold nanoparticles were fabricated by a gold etchant on silicon surface as SERS substrates and the optimized enhancement factor was determined to be 8.6×10^{6}. Zhong et al. [11] presented nanoparticles formed by $HAuCl_3$ and sodium citrate

solutions on the polymethyl methacrylate (PMMA) template as a transparent SERS substrate. Then, the malachite green with the concentration of 0.1nmol/L was detected using the AuNPs/PMMA film SERS substrates. Zhang et al. [12] fabricated the core-shell structure of SiO_2 and gold with sub-10nm shell thickness by adding $HAuCl_4$ and reducing agent K_2CO_3 solutions on the SiO_2 surface and found that the enhancement of SERS becomes weaker with the increase of shell thickness. However, nanoparticles fabricated by chemical synthesis method exists poor repeatability and uneven density, and the hot spot position is difficult to accurately determine.

Recently, all kinds of shapes of nanostructures were fabricated by several researchers as SERS substrates, including nanorod [14-16], nanostar [17,18], nanoantennas [19] and nanospheres [20] have been successfully machined by the existing lithography-based technologies. Furthermore, nanostructures are also fabricated by combination of lithography [21-25] methods and dry etching or wetting etching. For example, the commercial Klarite substrate [21-23] fabricated by electron beam lithography and wetting etching consists of square-based pyramidal pits with 1μm deep on the silicon surface. Then the rhodamine solution of 10^{-4}mol/L are detected by using the Klarite substrate. Candeloro et al. [24] used lithography and reactive ion etching to fabricate nanoholes with a diameter about 400nm and 50nm in depth. Subsequently, the nanoholes were transferred by peeling template method on the glass surface and the detection resolution of the R6G molecules was 10^{-6}mol/L using the substrate. However, the major limitations of lithography-based method is low efficiency and unsuitablility mass production and is difficult to machine more

complex nanostructures.

Recently, the tip-based micro/nanomachining method [26-30] has been used to fabricate SERS substrates. Compared to other methods, the characteristics of this method are mainly two advantages. Firstly, the wear of the tip can be neglected during machining on the metal surface due to the low hardness of metals (copper, aluminum). Secondly, the micro/nanomechanical machining method is ideal for the fabrication of micro/nanostructures due to it allows the control of normal force or displacement, and thus the depth of the micro/nanostructures is accurately achieved. Additionally, the micro/nanomechanical machining method is suitable to machine more complex micro/nanostructures. Therefore, the arrayed microcavities were machined by a tip-based indention method provided by us previously [31]. By changing the period of the force signal and the machining feed, the complex arrayed micro/nanocavities are formed on the Cu(110) plane. Then, Ag nanoparticles used by the method of chemical redox reaction were generated on the cavities and pile-ups of Cu(110) surface. The different structures of the silver nanoparticles and copper surface can be produced by changing the corrosion time and the R6G molecules have been chosen as adsorbed markers. Finally, the Raman intensities of malachite green molecules with low concentration are detected on the optimized hierarchical SERS substrates. Combining force modulation indentation with chemical reaction methods, the hierarchical substrates are not only included complex micro/nanostructures, but also Ag nanoparticles are generated on the Cu(110) surface. It is anticipated to discriminate pesticide residues or virus at very small quantity.

Results and Discussion

Study on fabrication of hierarchical SERS substrates

The single crystal copper (110) plane was used as the sample with the dimension of 5 mm×10 mm×1 mm. The complex micro/nanostructures are fabricated with different feeds (f_x, f_y) by indentation method. The structured Copper surface was cleaned with a large amount of alcohol followed by acetone. Then, the concentration of 10^{-1} mol/L hydrochloric solution was employed to treat the structured Cu(110) surface with 30 minutes to remove the oxide layer. The concentration of 10^{-4} mol/L $AgNO_3$ solution was employed to treat the Cu(110) surface with a specified time. The Ag nanoparticles were generated on the Cu(110) surface and surface cleaning was carried out further using deionized water to remove any residual $AgNO_3$ reagent and copper nitrate production. A stream of nitrogen was then used to dry the hierarchical substrate, as shown in Figure 1.

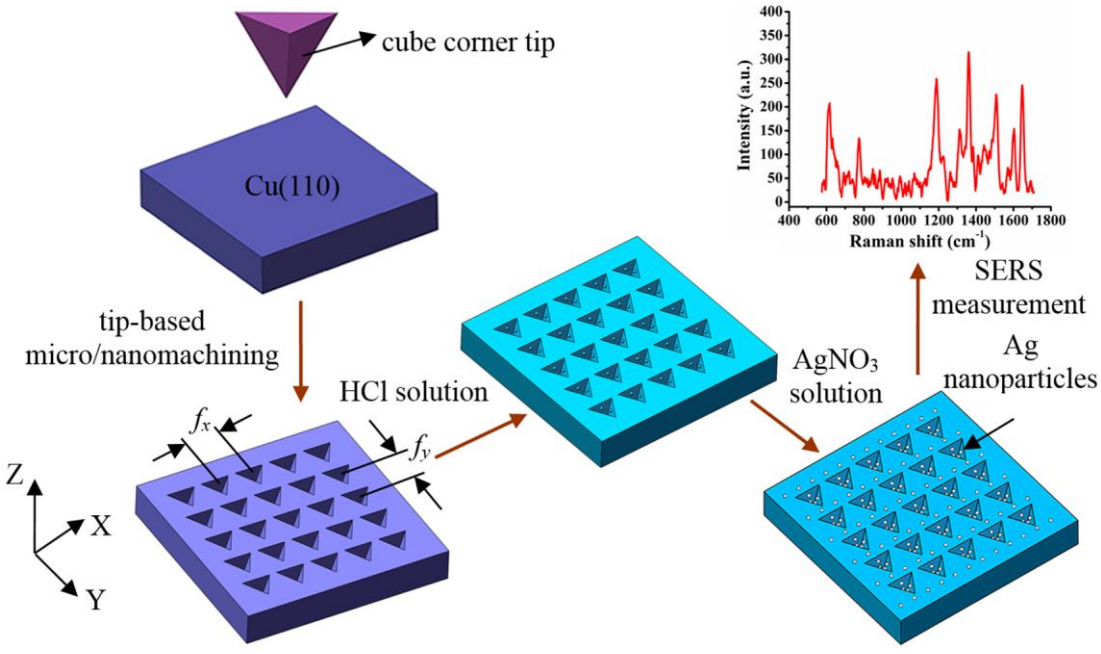

Figure 1 Schematic diagram of the hierarchical SERS substrate with Ag nanoparticles on the arrayed pyramid cavities

Hydrogen ions play an important role in the surface modification process since

they can effectively etch oxide layers e.g. making Cu(110) surface exposed to Ag+ at specific areas in equations (1) and (2). The reaction between Ag+ and Cu reacted in the cavities and Cu(110) surface and caused the formation of Ag nanoparticles.

$$CuO+2HCl=CuCl_2+H_2O \quad (1)$$

$$Cu+AgNO_3=CuNO_3+Ag \quad (2)$$

The SEM images of the arrayed triangular cavities fabricated by different feeds before and after the corrosion time of five minutes in $AgNO_3$ solution, as shown in Figure 2. Figure 2(a) shows the SEM images of arrayed triangular cavities with the f_x=5μm and f_y=1μm before the corrosions of HCl and $AgNO_3$ solutions. The triangular cavities are formed the structure of the similar "fish scale" with the f_x=5μm and f_y=1μm. Additionally, the inside of cavities and the surface of sample are smooth. However, the surface of sample, the inside of cavities and the pile-ups of materials are roughened using the HCl and $AgNO_3$ solutions, respectively. Furthermore, Ag nanoparticles are generated on the different positions, including the inside of cavities, pile-ups of materials and the surface of sample, as shown in Figure 2(b)-(e). Figure 2(b) shows the SEM images of arrayed triangular cavities etched by $AgNO_3$ solution with the f_x=2μm and f_y=1μm. The more complex structures are generated, due to the adjacent cavities overlapped and squeezed using the normal force control method with a decrease in feed (f_y). The nanoparticles are generated inside of the cavities and the pile-ups of the cavities using the $AgNO_3$ solution. The SEM images of arrayed pyramid cavities etched by $AgNO_3$ solution are formed with the f_x=2μm and f_y=2μm, as shown in Figure 2(c). The smaller pyramid cavities are formed by using the feed of 2μm in the two directions, respectively. The more Ag nanoparticles are generated on the smaller pyramid cavities. The adjacent cavities are just overlapped with the f_x=5μm and f_y=5μm, as shown in Figure 2(d). Compared to the inside of cavities, the more Ag nanoparticles are generated in the pile-ups of cavities. The “fish scale”

induced by machining are formed with the f_x=5μm and f_y=1μm, as shown in Figure 2(e). Compared to the original arrayed pyramid cavities, the structures of different positions are roughed using $AgNO_3$ solution. In addition, nanoparticles of the dimension of 200nm are formed in the different positions of cavities, as shown in Figure 2(e).

Figure 3 shows the SEM images of the arrayed triangular cavities machined by different feeds after the corrosion time of ten minutes in $AgNO_3$ solution. When the etching time is increased, the clustering structures are gradually generated due to the increase of dimension of Ag nanoparticles. Figure 3(a) shows the SEM images of arrayed triangular cavities with f_x=2μm and f_y=2μm at the etching time of 10 minutes in $AgNO_3$ solution. Compared to the pyramid cavities etched by 5 minutes, the topographies of pyramid cavities etched by 10 minutes are changed obviously, as shown in Figure 3(c). Figures 2(e) and 3(d) show the SEM images of arrayed triangular cavities with f_x=5μm and f_y=1μm. Compared to cavities etched by 5 minutes, more nanoparticles are generated in the cavities and pile-up of cavities and the clustering structures are formed in the pile-ups of cavities. The similar situation is happened with the feed of 5μm in the two directions, respectively. The nanoparticles etched by 5 minutes are only formed in the pile-ups of cavities, as shown in Figure 2(d).

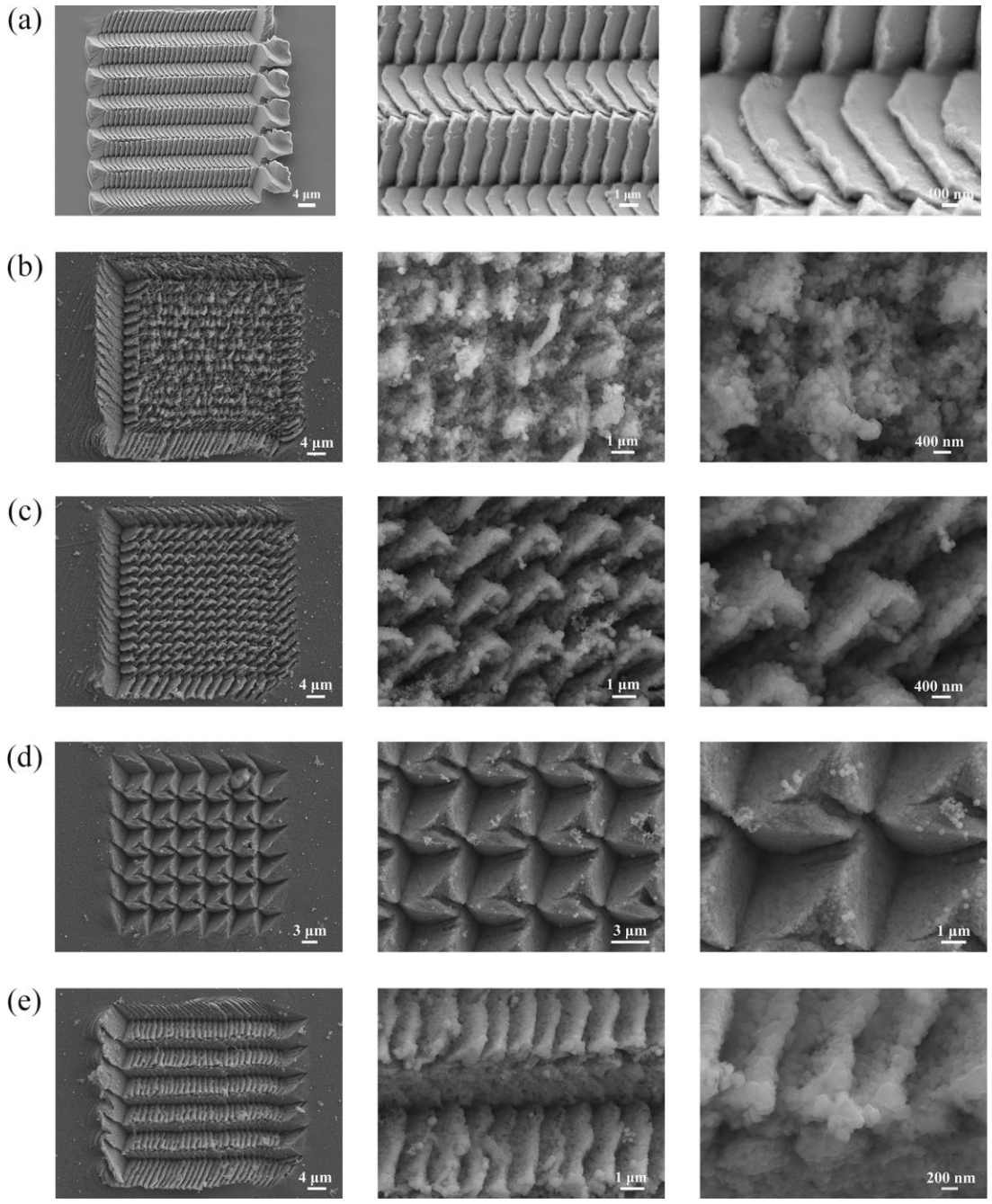

Figure 2 SEM images of the arrayed triangular cavities with different feeds in $AgNO_3$ solution before and after 5 minutes (a) f_x=5μm f_y=1μm before using $AgNO_3$ solution (b) f_x=2μm f_y=1μm after using $AgNO_3$ solution (c) f_x=2μm f_y=2μm (d) f_x=5μm f_y=5μm (e) f_x=5μm f_y=1μm.

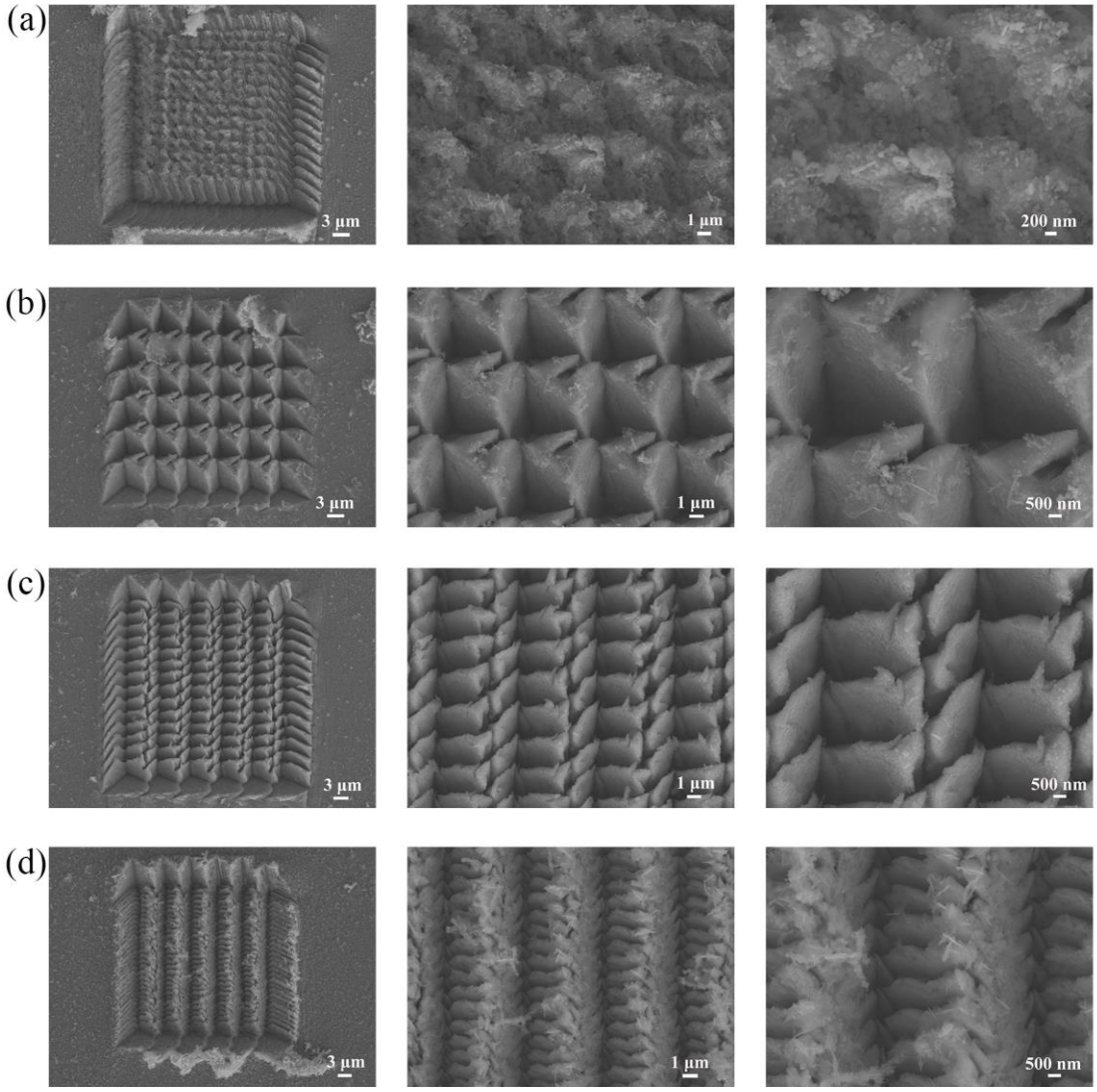

Figure 3 SEM images of the arrayed triangular cavities with different feeds in $AgNO_3$ solution with 10 minutes (a) f_x=2μm f_y=2μm (b) f_x=5μm f_y=5μm (c) f_x=5μm f_y=2μm (d) f_x=5μm f_y=1μm.

Analysis of Ag nanoparticles in the arrayed pyramid cavities

Figure S1 shows the SEM and EDS images of Ag/Cu substrates etched by 5 minutes in ESI†, respectively. Nanoparticles are generated on the Cu(110) plane, as shown in Figure S1(a). The elements of hierarchical surface contain copper, silver and oxygen, as shown in Figure S1(b). Copper is main element of substrate and Ag is formed on the Cu substrate due to redox reaction. Oxygen is generated with the Ag nanoparticles formed. The mass ratio of Ag nanoparticles is 0.66% and the atomic ratio is 0.35% for the mass ratio of total element, as shown in table S1 in ESI†.

Figure S2 shows SEM and EDS images of the triangular cavities with f_x=5μm、

f_y=1μm in $AgNO_3$ solution with 5 minutes, respectively. Figures S2(a) and (b) show SEM images of structures like “fish scale” formed by the deformation of adjacent cavities and pile-ups of cavities. The elements of copper, silver and oxygen are generated in the cavities and pile-ups of cavities, as shown in Figs. S2(c) and (d) in ESI†. Tables S2 and S3 show the distribution of the contents of each element on the inside of internal cavities and pile-ups of cavities with f_x=5μm and f_y=1μm, respectively. Compared to other elements, the mass and atomic ratio of copper are higher because it is the base of substrate. The mass ratio of silver is 10.43% on pile-ups of cavities. However, the mass ratio of silver is only 0.62% on the inside of cavities. Therefore, the contents of silver on the pile-ups of cavities is higher than the content of silver on the inside of cavities and the content of mass ratio is about 16 times. The atomic ratios of silver are 4.11% and 0.23% on the pile-ups of cavities and inside of cavities, respectively. Therefore, the content of silver on the pile-ups of cavities is about 17 times on the inside of cavities.

Figure S3 shows SEM and EDS images of the arrayed triangular cavities with f_x=2μm、f_y=2μm in $AgNO_3$ solution with 5 minutes, respectively. Tables S4 and S5 show the distribution of the contents of each element of the internal cavities and pile-ups of cavities with f_x=2μm and f_y=2μm, respectively. The mass ratio of silver is 10.25% on the pile-ups of cavities. However, the mass ratio of silver is only 0.64% on the inside of cavities. The atomic ratios of silver are 4.12% and 0.25% on the pile-ups of cavities and inside of cavities, respectively. It is demonstrated that the contents of silver on the pile-ups of cavities is higher than the content of silver on the inside of cavities. The contents of silver are consistent on the pile-ups of cavities with f_x=5μm, f_y=1μm and f_x=2μm, f_y=2μm, as shown in Tables. S3 and S5 in ESI†.

Figure S4 shows SEM and EDS images of the arrayed triangular cavities with

f_x=5μm、f_y=5μm in $AgNO_3$ solution with 5 minutes in ESI†, respectively. Figures S4(a) and (b) show SEM images of two adjacent cavities and the pile-ups of cavities with f_x=5μm、f_y=5μm, respectively. Similar conclusions are obtained for different arrayed pyramid cavities with different feeds. The content of Ag nanoparticles with pile-ups of cavities is higher than the content of the internal cavities, as shown in Figs. S4(c)-(d). Tables S6 and S7 show the contents of each element of the internal cavities and pile-ups of cavities with f_x=5μm and f_y=5μm, respectively. The mass ratio of silver is 4.03% on the pile-ups of cavities. However, the mass ratio of silver is only 0.77% for the internal cavities. The atomic ratios of silver are 1.65% and 0.3% on the pile-ups of cavities and internal cavities, respectively. Compared to other structures with different feeds, such as f_x=5μm、f_y=1μm, f_x=2μm、f_y=2μm, the content of Ag nanoparticles is lower on the pile-ups of cavities with f_x=5μm、f_y=5μm, as shown in Tables S3, S5 and S7 in ESI†.

The study of the arrayed pyramid fabricated by different feeds indicates that the Ag nanoparticles formed on the internal cavities and pile-ups of cavities are much more higher than Ag nanoparticles formed on the plane during chemical corrosion. The stress of cavities and plane are different due to the pile-ups of material generated during fabricating arrayed pyramid cavities. The changes of stress state on the different positions are a significant effect for the result of chemical corrosion. Additionally, the deformation of material and defection of structures are caused due to the generation of stress during machining arrayed pyramid cavities. On the one hand, the replacement reaction are achieved in the single crystal copper surface and the $AgNO_3$ solution and Ag nanoparticles are formed on the different positions of single crystal copper surface. On the other hand, the single crystal copper surface becomes rougher and more defects are formed after the etching process. Furthermore, the

defects of the internal cavities and pile-ups of cavities are much higher than the surface of single crystal copper. Compared to single crystal copper surface, the internal cavities and pile-ups of cavities are easier etched by $AgNO_3$ solution. Therefore, the stress state affects the corrosion structure. Compared to the single crystal copper surface, the more silver nanoparticles are formed in the internal cavities and pile-ups of cavities.

The Raman intensity on structured Ag/Cu hierarchical substrates

(1) Optimization of mircostructures with different machining parameters for hierarchical SERS substrates

The arrayed triangular cavities with different $AgNO_3$ solution corrosion time and different machining parameters have a significant influence for the performance of hierarchical SERS substrates. R6G is employed as the Raman probe molecules to research the Raman enhancement performance. Thus, the Raman detection is performed for hierarchical SERS substrates with different machining parameters and corrosion time.

Figure 4 shows SEM image of single cavity of Ag/Cu substrate with f_x=10μm and f_y=10μm and Raman spectrum of R6G molecules of 10^{-8}mol/L on the single Ag/Cu substrate, respectively. A and B represent pile-ups of cavity and the interval cavity for the single cavity, respectively, as shown in Figure 4(a). Figure 4(b) shows Raman spectrum images of R6G molecules in the pile-ups of cavities and the interval cavity, respectively. Compared to the Raman intensity of R6G molecules in the internal cavity, it exhibit a stronger enhancement in the pile-ups of cavity.

The parameters of the feeds(f_x、f_y) for fabricating micro/nanostructures using the method presented are shown to research the effect of Raman enhancement of R6G molecules in Table S8 in ESI†.

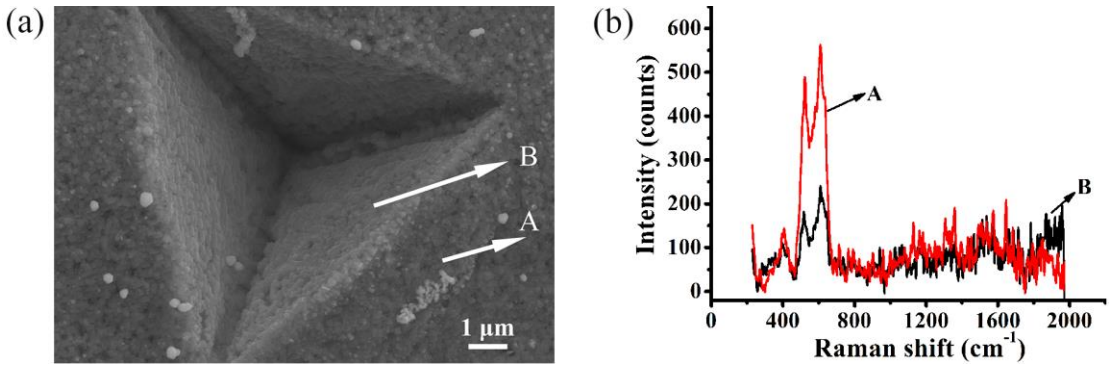

Figure 4 (a) SEM image of the single Ag/Cu pyramid substrate with the feed of f_x=10μm、f_y=10μm. (b) Raman spectrum of R6G molecules of 10^{-8}mol/L on the single Ag/Cu substrate.

Figure S5 shows the Raman spectrum of R6G molecules of 10^{-8}mol/L for hierarchical SERS substrates with the corrosion time of 5 minutes in $AgNO_3$ solution. The Raman peaks of R6G molecules were indentified at 611, 772, 1183, 1312, 1362, 1504 and 1604 cm^{-1} on the different hierarchical substrates, as shown in Figure S5(a). Figure S5(b) shows the average Raman intensity of R6G of the 1362 cm^{-1} peak of the arrayed triangular cavities with different feeds at the corrosion time of 5 minutes in $AgNO_3$ solution, corresponding to Figure S5(a).

When the feed in the two directions ranges from 5-3μm, the Raman intensities do not change significantly, as shown in Figure S5(b). However, compared to other machining parameters, the Raman intensity of R6G molecules exhibits a stronger enhancement with three hierarchical structures, including (6), (9) and (10), as shown in Figure S5(b). On the one hand, the "fish scale" structures are formed due to adjacent cavities overlapped and squeezed. Compared to the Raman intensity of R6G molecules in the plane, it generates a stronger enhancement for the "fish scale" structures. On the other hand, compared to other structures, more Ag nanoparticles are generated on the "fish scale" structures using two parameters, as shown in Figures S2 and S3 in ESI†. The higher content of Ag element indicates the more nanoparticles formed in the pyramid cavities and the stronger electric field is generated between the nanoparticles. Therefore, the higher Raman intensity of R6G molecules is detected on

the “fish scale” structure.

(2) Effect of Raman enhancement performance of hierarchical SERS substrates with different corrosion time

In order to reserach the effect of Raman enhancement of the hierarchical SERS substrate with different corrosion time, the structured single crystal copper was immersed in $AgNO_3$ solution for 10 minutes with the concentration of 10^{-3} mol/L. The substrate was then dried using a stream of nitrogen and was soaked in R6G solution of 10^{-8} mol/L for 2h. When the same laser intensity of 2.39mW(10%) with the etching time of 5 minutes is chosen, the Raman peaks of carbon is generated and the Raman peak of R6G molecules is not detected with the etching time of 10 minutes. The R6G molecules are carbonized due to the excessive Raman intensity. Thus a small laser intensity of 0.016mW(0.1%) is used to detect the Raman intensity of different hierarchical SERS substrates. Figure S6 shows the Raman spectrum of the R6G molecules of 10^{-8} mol/L for hierarchical SERS substrates with the corrosion time of 10 minutes in $AgNO_3$ solution. When the smaller laser intensity is employed, the Raman intensity of R6G molecules is not detected for the structures with other machining parameters. However, the Raman intensities of R6G molecules are detected, when f_x is 2μm and f_y ranges from 3μm-1μm, as shown in Figure S6(a) in ESI†. Compared to the other machining feeds, the Raman intensity of R6G molecules is the largest with f_x=2μm and f_y=2μm. Additionally, the Raman intensity with the pile-ups of cavities is ten times larger than the Raman intensity with the internal cavities, as shown in Figure S6(b) in ESI†.

On the one hand, compared to the internal cavities, the Raman intensity can be enhanced due to more Ag nanoparticles generated in the pile-ups of cavities. It is indicated that Ag nanoparticles are favorable to form on the pile-ups of cavities for the

hierarchical substrates. On the other hand, Ag nanoclusters are formed on the pile-ups of cavities with increasing of the corrosion time in $AgNO_3$ solution, as shown in Figures 3(a) and (b). The Raman intensity can be enhanced further due to the formation of nanoclusters. Other scholars have already obtained similar conclusions [10,17,32]. Copper nanowires are soaked in AgNO3 solution by Wang et al. [10] and Ag nanoparticles are generated with the dimension of 25nm on the surface of copper nanowires. Therefore, the properties of nanowires are significantly improved, including electrical, optical and mechanical characteristic. A local electric field enhancement is caused by a single nanoparticle contacted with the sample and the "hot spots" are formed by multiple nanoparticles to improve electric field intensity and local electromagnetic field. Therefore, the Raman intensities of molecules absorbed on the surface of nanoparticles are enhanced by the local electric fields. Zhang et al. [32] deposited a Ag film of 30 nm and a Au film of 10 nm on the roughened silicon surface by thermal evaporation method, respectively. The higher Raman intensity was detected on the Au@Ag particles and the R6G molecules solution with the concentration of 10^{-8} mol/L was detected using this substrate. A three-dimensional nanostar structure was fabricated by Gopalakrishnan et al. [17] in a circular groove. The electric field intensity was greatly improved by the adjacent nanostars and the adenine molecules were detected with low concentration. Compared to the results of other scholars, Ag nanoparticles are fabricated by the redox reaction or physical deposition methods by scholars. Multiple Ag nanoparticles are formed to improve further the Raman intensity of probe molecules. However, the difference for the conclusions obtained by other scholars is that the Raman intensities of different positions of arrayed pyramid cavities fabricated by the force-controlled indentation machining method are different, including the internal cavities and the pile-ups of

cavities. Moreover, the Raman intensities detected by arrayed pyramid cavities with different machining feeds are also different.

(3) Study on Surface enhanced Raman properties of hierarchical structures based on finite element simulation

In order to further verify the effect of the electric field intensity of the hierarchical structures and comprehend the enhancement mechanism of the AgNPs/Cu nanostructures. The local electric field of the AgNPs/Cu nanostructures calculated using commercial COMSOL software. Figure S7 shows the x-z views of single Ag nanoparticle of the electric field distribution on the air and Cu surface with incident wavelength 532 nm, respectively. The definitions of the geometrical parameters are provided: E(x), H(y) and K(z) are the electric field, magnetic field and direction of light propagation, respectively. The electric field intensity is 2.19V/m with the radius of Ag nanoparticle of 100nm in the air, as shown in Figure S7(a) in ESI†. Figure S7(b) shows the electric field distribution of a Ag nanoparticle with a radius of 100nm on the Cu substrate. The maximum value of the electric field intensity is mainly concentrated on the contact between copper surface and the silver particle and the electric field intensity is 16.734V/m. It indicates that electric field coupling occurs between the copper substrate and the Ag nanoparticle and a new “hot spot” is formed.

Figure 5 shows the electric field distribution of a single/three adjacent silver particles with a radius of 100 nm on a pile-up of copper substrate. Figure 5(a) shows the electric field distribution of hierarchical structure with a pile-up of copper structure and a single silver nanoparticle. A hot spot is generated between the pile-up of copper substrate and the silver particle, and the electric field intensity is 38.899V/m. Compared to individual silver nanoparticles on the copper surface, the electric field

intensity of a single silver particle contacted on the pile-up structure is increased by a factor of about three. Figure 5(b) is a electric field distribution of hierarchical structures with a pile-up of copper structure and adjacent silver nanoparticles cluster structures, where the scale is set to log|E/E0|. A new hot spot is generated due to the interaction with adjacent Ag nanoparticles. At the same time, the other hot spot between the Ag nanoparticle and the pile-up of Cu structure is formed and the SERS hot spot intensity is greatly enhanced. The electric field intensity of three adjacent Ag nanoparticle cluster structures on the pile-up of Cu substrate is 380V/m. Compared to a single Ag nanoparticle on the pile-up of Cu substrate, the electric field intensity is greatly enhanced further. In addition, the simulation model corresponds to the SEM topographies of the indentation structures fabricated by different feeds in the $AgNO_3$ solution with 5 minutes, as shown in Figures. S2(a) and S4(a). The Ag nanoparticles are formed on the pile-ups of the indentation structures and the adjacent nanoparticles with the radius of 100nm are contacted with each other, which corresponds to the simulation model. The simulation results in this section are consistent with the Raman intensities of the R6G molecules detected on the different triangular cavities in the experiment, as shown in Figure S5(b). Just discussed above, the EM is generated from metal nanoparticles, once attaching the AgNPs on the pile-up of copper surface, electrical field intensity of the plasmonic resonance can be effectively amplified and increased.

According to the above research, the SERS behaviors of the AgNPs/pyramid hierarchical substrates can contribute to the following points: (1) the pyramidal cavities and pile-up of copper substrate can be employed as the amplifer and induced large electrical field intensity of the plasmonic resonance. (2) The adjacent AgNPs can be generated an extra electrical field enhancement. The AgNPs/pyramid hierarchical

SERS substrates with higher sensitivity can be achieved based on theoretical results. Therefore, the combination of Ag nanoparticles clusters on the pile-up of copper surface forms a new nanogap and improves the density of SERS hotspots. Compared to the hierarchical substrate on the copper plane, the electric field intensity of hierarchical substrate on the pile-ups of copper surface is higher.

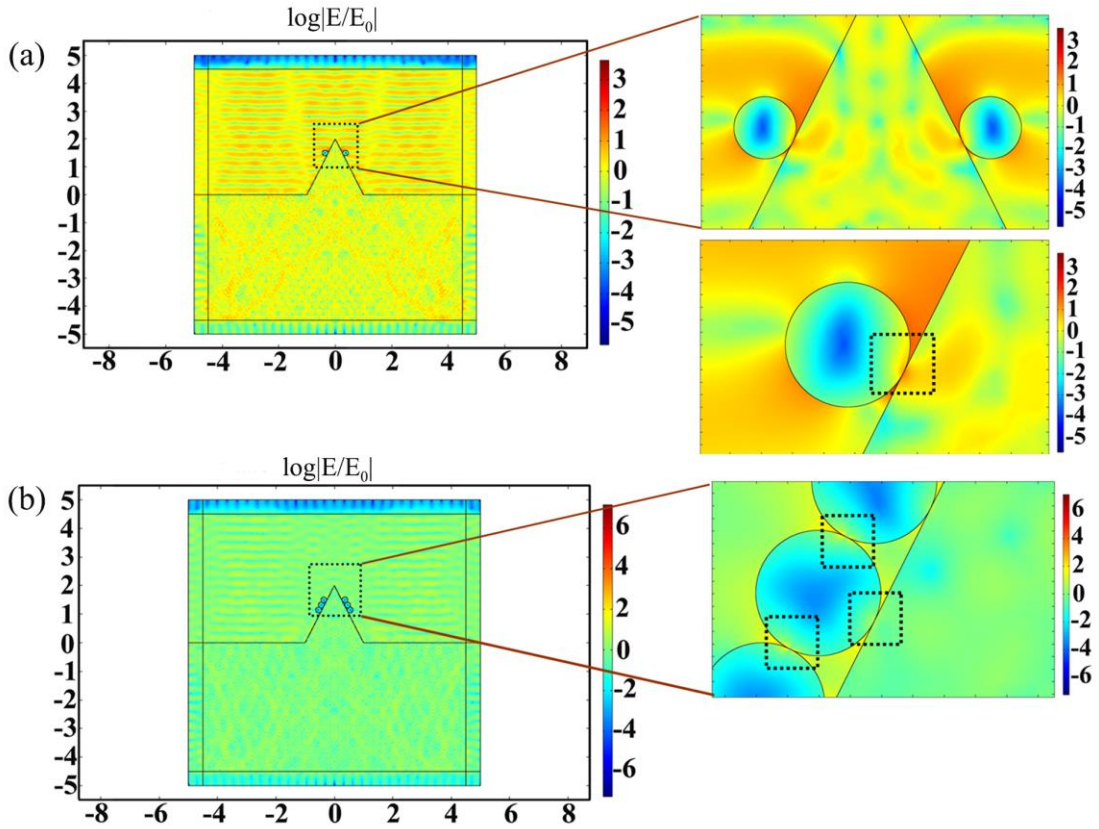

Figure 5(a) Electric field distribution of single Ag nanoparticle with the radius of 100nm on the pile-up of Cu substrate (b) Electric field distribution of three Ag nanoparticles with the radius of 100nm on the pile-up of Cu substrate.

(4) Study on the Raman intensity of Malachite Green molecules for hierarchical SERS substrates

Malachite Green commonly is used in food and biological dyes in the industry and is also one of the most commonly bactericide in fishery. However, malachite green is highly toxic for aquatic animals or mammals and can be induced cancer for the animals. Thus the MG is significantly detected with low concentration in water. The content of malachite green can not be higher than 2μg/kg (5.48×10^{-9}mol/L) for

many national food safety standards. Pesticide residues of food are detected by using many methods, including gas chromatography, gas chromatography-mass spectrometry and liquid chromatography. Although these methods have the advantages with high detection accuracy, the disadvantages of these methods are included complicated preprocessing and the detection with a long time. However, SERS technology is a new choice to detect pesticide residue with fast, simple and high sensitivity.

The characteristic Raman peaks of Malachite Green molecules were indentified at 1172, 1219, 1364, 1394, 1586 and 1614 cm^{-1} on the different hierarchical substrates, as shown in Figure 6.

The incident optical power was 0.148 mW (1%) in the experiment. In this section, the structure of the Ag/Cu substrate obtained by etching in $AgNO_3$ solution for 10 minutes is used to detect malachite green molecules with a concentration of 10^{-7}mol/L, as shown in Figure 6. Figure 6(a) shows the Raman spectrums of the MG molecules for hierarchical SERS substrates with the different feeds. Compared to the other indentation structures, the Raman intensity of MG molecules is weak with the separated indentation structures. The Raman intensity of other hierarchical SERS structures gradually increases with the decrease of feed.

Figure 6(b) shows the average Raman intensity of MG molecules of the 1614cm^{-1} peak in the Ag/Cu structures with the different feeds. The Raman intensity of MG molecules is 40±10 counts with the separated indentation structures. When the feed of the y direction ranges from 5μm to 1μm, the Raman intensities gradually increase. Similar to the detection of R6G molecules, the Raman intensities of the three structures are higher than that of structures fabricated by other parameters for the MG molecules, including (6), (9) and (10). The "fish scale" structure formed with f_x=5μm

and f_y=1μm and f_x=2μm and f_y=1μm, respectively. The other indentation structures are the formed by the extrusion deformation of the indentation with the feed of 2μm of X direction and 2μm of Y direction, as shown in Figure 3. In particular, the Raman intensity of malachite green is the largest with the feed of 2μm of X direction and 2μm of Y direction. The conclusion of detection of MG molecules is similar to the detection of R6G molecules.

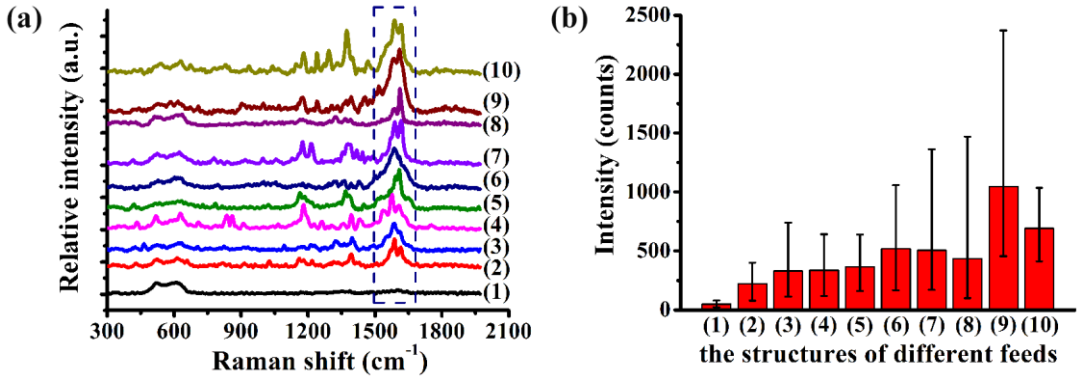

Figure 6 Raman spectrum of MG molecules of 10^{-7}mol/L on Ag/Cu substrates with the corrosion time of 10 minutes. (a) Raman spectrums of the MG molecules for hierarchical SERS(Ag/Cu) substrates with the different feeds. (b) Average Raman intensity of MG molecules of the 1614cm^{-1} peak in the Ag/Cu structures with the different feeds.

The machining parameter is the feed of 2μm of X direction and 2μm of Y direction and the corrosion time is 10 minutes in the $AgNO_3$ solution as the hierarchical substrate. The detection limit of MG solution is studied for the enhancement performance of hierarchical SERS substrate with the concentrations of 10^{-7}mol/L and 10^{-9}mol/L. The malachite green molecules at a concentration of 10^{-9}mol/L are detected using the determined optimal processing structure to confirm whether the hierarchical structures can meet the requirements of standard. The detection limit of the hierarchical SERS substrate is 10^{-9}mol/L and meets the requirement of national standard (5.48×10^{-9}mol/L), as shown in Figure 7.

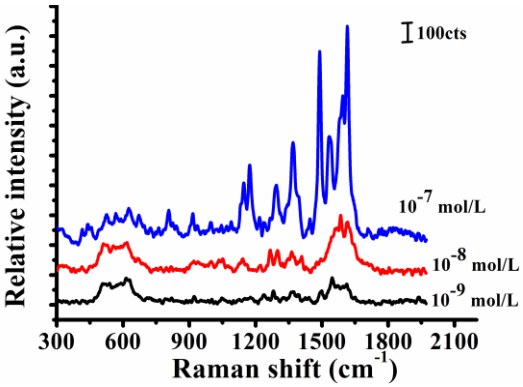

Figure 7 Raman spectrum of MG molecules on Ag/Cu substrates with different concentrations

Conclusions

A novel method based on indentation and chemical redox reaction is proposed to fabricate the hierarchical SERS substrates for the detection of the probe molecules with high resolution. Firstly, compared to the different corrosion time of $AgNO_3$ solution, the optimal corrosion time of $AgNO_3$ solution is 10 minutes, which renders the more number of silver nanoparticles on the indentation surface. Secondly, compared to the Raman intensities on the internal cavities，the Raman intensities on the pile-ups of materials is higher through the analysis of energy spectrum and Raman spectrum due to Ag nanoparticles easily generated on the pile-ups of materials. In addition, the Raman intensity of R6G is higher with the feed of 2μm of X direction and the feed of 2μm of Y direction on the different indentation structures. Thirdly, the intensity and distribution of electric fields of Ag nanoparticles used by comsol software are shown in the plane substrate and cavities substrate, respectively. Compared to the intensity of electric field of Ag nanoparticles on the plane substrate, the electric field intensity of Ag nanoparticles on the pile-ups of materials is higher. The new hot spots are formed at the gap between the adjacent Ag nanoparticles and between Ag nanoparticles and the pile-ups of materials, respectively. Finally, the

malachite green molecules commonly used in aquatic products are detected by the proposed method. This method can meet the requirements of standard and the enhancement factor of malachite green molecules is 5.089×10^{9} using the optimal indentation structures.

Experimental Section

In this experiment, an EDX instrument (Zeiss, Germany), which was employed to identify the elemental composition of substrates, was equipped to the SEM which was employed to prove that the silver had been generated on the copper surface. The micro-Raman spectroscopic system (Renishaw, inVia, UK) was equipped with a 532 nm wavelength and focused with a 50× objective lens. The incident optical power was set up to be 0.6 mW and the beam diameter was about 1 μm. The signal detector was employed a Renishaw CCD camera (1040×256). At the beginning of the tests, the Raman spectrum was rectified by a standard Si substrate, without finding specific peaks. The Raman intensity R6G probe peak and Malachite green molecules peak were chosen as 1362 cm^{-1} or 1614 cm^{-1}, which are the major Raman peak for R6G molecules and MG molecules, respectively.

Conflicts of interest

The authors declare no competing financial interest.

Supporting Information

Acknowledgements

The research in this paper was sponsored by National Natural Science Foundation of China (grant No. 51905047, 51675134, 21827802, 51575057) and Jilin Province

Science and Technology Project (grant No. 20170101124JC).

References

1. McHugh, K. J.; Nguyen, T. D.; Linehan, A. R.; Yang, D.; Behrens, A. M.; Rose, S.; Tochka, Z. L.; Tzeng, S. Y.; Norman, J. J.; Anselmo, A. C. *Science* **2017**, 357, 1138–1142. doi:10.1126/science.aaf7447

2. Salerno, M.; Shayganpour, A.; Salis, B.; Dante, S. *Beilstein J. Nanotechnol*. **2017**, 8, 74–81. doi:10.3762/bjnano.8.8

3. Amendola, V. *Beilstein J. Nanotechnol.* **2019**, 10, 1016–1023. doi: 10.3762/bjnano.10.102

4. Zhang, X. G.; Zhang, X. L.; Luo, C. L.; Liu, Z. Q.; Chen, Y. Y.; Dong, S. L.; Jiang, C. Z.; Yang, S. K.; Wang, F. B.; Xiao, X. H. *Small* **2019**, 15, 1805516. doi:10.1002/smll.201805516

5. Zhang, C.; Man, B. Y.; Jiang, S. Z.; Yang, C.; Liu, M.; Chen, C. S.; Xu, S. C.; Qiu, H. W.; Li, Z. *Appl. Surf. Sci.* **2015**, 347, 668–672. doi:10.1016/j.apsusc.2015.04.170

6. Yang, H; Ni, S. Q.; Jiang, X. H.; Jiang, W.; Zhan, J. H. *CrystEngComm*. **2012**, 14, 6023–6028. doi:10.1039/c2ce25609f

7. Morton S. M.; Jensen L. *J. Am. Chem. Soc*. **2009**, 131, 4090–4098. doi:10.1021/ja809143c

8. Chen L. Y.; Yu J. S.; Fujita T.; Chen M. W. *Adv. Funct. Mater.* **2009**, 19, 1221–1226. doi: 10.1002/adfm.200801239

9. Lin, H. Y.; Shao, Q; Hu, F; Wang, H; Shao, M. W. *Thin Solid Films* **2014**, 558, 385–390. doi:10.1016/j.tsf.2014.02.057

10. Zhang, X. M.; Guo, L; Luo, J. M.; Zhao, X. Q.; Wang, T. Q.; Li, Y. N.; Fu, Y. *ACS Appl. Mater. Interfaces* **2016**, 8, 9889–9896. doi:10.1021/acsami.6b01658

11. Zhong, L. B.; Yin, J; Zheng, Y. M.; Liu, Q.; Cheng, X. X.; Luo, F. H. *Anal. Chem.* **2014**, 86, 6262–6267. doi:10.1021/ac404224f

12. Zhang, L; Guan, C. R.; Wang, Y.; Liao, J. H. *Nanoscale* **2016**, 8, 5928–5937.

13. Li, J. F.; Zhang, Y. J.; Ding, S. Y.; Panneerselvam, R; Tian, Z. Q. *Chem. Rev.* **2017**, 117, 5002–5069.

14. Shanmukh, S.; Jones, L.; Driskell, J.; Zhao, Y., Dluhy, R., Tripp, R. A.; *Nano lett.* **2006**, 6 2630–2636. doi:10.1021/nl061666f

15. Dai, Z. G.; Xiao, X. H.; Wu, W; Liao, L; Mei, F; Yu, X. F.; Guo, S. S.; Ying, J. J.; Ren, F; Jiang, C. Z. *Appl. Phys. Lett*. **2014**, 105, 211902. doi:10.1063/1.4902812

16. Alsammarraie, F. K.; Lin, M. *J. Agric. Food Chem*. **2017**, 65, 666–674. doi:10.1021/acs.jafc.6b04774

17. Gopalakrishnan, A.; Chirumamilla, M.; De Angelis, F.; Toma, A.; Zaccaria, R. P.; Krahne, R. *ACS nano* **2014**, 8, 7986–7994. doi:10.1021/nn5020038

18. Chirumamilla, M.; Gopalakrishnan, A.; Toma, A.; Zaccaria, R. P.; Krahne, R. *Nanotechnology* **2014**, 25, 235303. doi:10.1088/0957-4484/25/23/235303

19. Huck, C.; Toma, A.; Neubrech, F.; Chirumamilla, M.; Vogt, J.; De Angelis, F.; Pucci, A. *ACS Photonics* **2015**, 2, 497–505. doi:10.1021/ph500374r

20. Yockell-Lelièvre, H.; Lussier, F.; Masson, J. F.; *J. Phys. Chem. C* **2015**, 119, 28577–28585. doi:10.1021/acs.jpcc.5b09570

21. Scholes, F. H.; Davis, T. J.; Vernon, K. C.; Lau, S. A.; Furman, S. A.; Glenn, A. M. *J. Raman Spectrosc*. **2012**, 43, 196–201. doi: 10.1002/jrs.3034

22. Mabbott, S.; Xu, Y.; Goodacre, R. *Anal. Methods* **2017**, 9, 4783–4789. doi:10.1039/c7ay01584d

23. Zhu, S. M.; Fan, C. Z.; Wang, J. Q.; Liang, E. J.; Hao, H. S. *Spectrosc. Lett*. **2018**, 51, 453–461.

doi:10.1080/00387010.2018.1503603

24. Candeloro, P.; Iuele, E.; Perozziello, G.; Coluccio, M. L.; Gentile, F.; Malara N.; Mollace, V.; Fabrizio, E. D. *Microelectron. Eng*. **2017**, 175, 30–33. doi: 10.1016/j.mee.2016.12.015

25. Geng, Y. Q.; Yan, Y. D.; Wang, J.Q.; Zhuang, Y. *Nanomanufacturing and Metrology* **2018**, 1, 225–235. doi: 10.1007/s41871-018-0024-9

26. Yao, C. K.; Liao, J. D.; Lin, C. H.; Yang, Y. S.; Yu, S. H.; Yang, J. W. *Sens. and Actuators B* **2014**, 191, 219–226. doi: 10.1016/j.snb.2013.09.120

27. Zhang, J. R.; Yan, Y. D.; Hu, Z. J., Zhao, X. S. *Proc. Inst. Mech. Eng., Part B* **2018**, 232, 1928–1942. doi: 10.1177/0954405416682276

28. Zhang, J. R.; Yan, Y. D.; Hu, Z. J.; Zhao, X. S. *Proc. Inst. Mech. Eng., Part B* **2018**, 232, 1310–1315. doi: 10.1177/0954405416666908

29. Maculotti, G.; Genta, G.; Lorusso, M.; Pavese, M.; Ugues, D.; Galetto, M. *Nanomanufacturing and Metrology* **2019**, 2, 16–25. doi: 10.1007/s41871-018-0030-y

30. Galetto, M.; Maculotti, G.; Genta, G.; Barbato, G.; Levi, R. *Nanomanufacturing and Metrology* **2019**, 2, 91–99. doi: 10.1007/s41871-019-00035-5

31. Yan, Y. D.; Zhang, J. R.; Xu, P.; Miao, P. *RCS Adv*. **2017**, 7, 11969–11978. doi: 10.1039/c6ra28875h

32. Zhang, C.; Jiang, S. Z.; Yang, C.; Li, C. H.; Huo, Y. Y.; Liu, X. Y.; Liu, A. H.; Wei, Q.; Gao, S. S.; Gao, X. G.; Man, B. Y. *Sci. Rep*. **2016**, 6, 25243. doi: 10.1038/srep25243